A Unified TLM Model for Wave Propagation of Electrical and Optical Structures Considering Permittivity and Permeability Tensors

Jifu Huang and Ke Wu, *Senior Member, IEEE*

***Abstract*—A generalized transmission line matrix (TLM) formalism is proposed for unified simulation of wave propagation problems. The present modeling is made possible with a new TLM node that is derived to account for simultaneously the electromagnetic effects of permittivity and permeability tensors of material. It is shown, through numerical examples, that the new node-based TLM algorithm in the frequency domain can be used to solve a large class of complex electromagnetic problems ranging from microwave circuits to optical devices. A dynamic solution for the r-cut sapphire-based microstrip is presented that highlights its application to high-temperature superconducting microwave circuits.**

I. Introduction

IT HAS BEEN recognized that various electromagnetic materials are always the cornerstone for the development of integrated structures ranging from radio-frequency (RF), microwave to optical circuits. With ever-increasing complexity of geometry and material property, designing these circuits requires more and more sophisticated field theoretical-based tools to predict their electrical and/or optical characteristics. Usually, such CAD tools should precisely account for any possible parametric effect of structure at a given frequency so that the length of design cycle and the cost related to experiments as well as the tuning procedure of post-fabrication could be minimized.

Much work in the field of CAD that has been done so far is mainly concerned with wave propagations under the consideration or assumption of isotropic or diagonal tensor property of material. This scenario is in fact related to and also limited by the computational problem of the modeling technique used in the CAD. Unfortunately, a lot of circuit materials exhibit more and less anisotropic behavior under certain circumstances that cannot be ignored in the circuit simulation. This is in particular important for a class of microwave and optical materials, sapphire substrate for high-temperature superconducting circuits [1], [2], $LibNO_3$ waveguide for electro-optical devices [3], [4], to name two examples. Nonreciprocal microwave devices [5] opt to deal with anisotropic medium such as ferrite which exhibits Hermitian-type permeability tensor. Obviously, an accurate theoretical characterization involving arbitrary tensors is the bottleneck for successful design and applications of anisotropic material-based circuits and devices. A unified field modeling is highly preferred that is able to consider generalized tensor conditions and also to handle irregular geometry of structure.

The transmission line matrix (TLM) technique [6]–[8] is well known for its capability in treating a wide range of electromagnetic problems with a great flexibility in terms of geometrical irregularity and material parameters. The equivalence between Maxwell's equation and circuit network allows this technique to solve complex problems in both time- and frequency-domains [9], [10]. This is done with a number of hybrid and condensed nodes [11]–[14], notably, the symmetrical condensed node (SCN). The SCN was initially proposed to handle isotropic and nondispersive materials. A subsequent extension has made it possible to include the diagonal anisotropic and dispersive properties of material [15], [16].

In this paper, a generalized TLM node is proposed and formulated to account for both arbitrary permittivity and permeability tensors. Using the present node, a frequency domain TLM algorithm is derived to address various computational issues of nondiagonal tensor problems encountered in the practical situations. Numerical examples are presented for two case studies: Rectangular waveguide partially filled with magnetized ferrite and microstrip line deposited on m-cut and r-cut sapphire substrates. Thus, the usefulness of the proposed modeling is verified and also highlighted by its application of a hybrid-mode analysis to the sapphire-based high-temperature superconducting microwave integrated circuits.

II. Theory

A. Generalized TLM Node Formulation

The generalized tensors $\overleftrightarrow{\varepsilon}$ and $\overleftrightarrow{\mu}$ for an anisotropic medium in a rectangular Cartesian coordinate can be expressed in the following form

$$\overleftrightarrow{\varepsilon} = \varepsilon_0 \cdot \begin{bmatrix} \varepsilon_{xx} & \varepsilon_{xy} & \varepsilon_{xz} \\ \varepsilon_{yx} & \varepsilon_{yy} & \varepsilon_{yz} \\ \varepsilon_{zx} & \varepsilon_{zy} & \varepsilon_{zz} \end{bmatrix},$$

$$\overleftrightarrow{\mu} = \mu_0 \cdot \begin{bmatrix} \mu_{xx} & \mu_{xy} & \mu_{xz} \\ \mu_{yx} & \mu_{yy} & \mu_{yz} \\ \mu_{zx} & \mu_{zy} & \mu_{zz} \end{bmatrix}. \quad (1)$$

Manuscript received January 30, 1995; revised June 29, 1995.

The authors are with The Research Center for Advanced Microwave and Space Electronics (Le Centre Poly-Grames), Department de Génie Électrique et de Génie Informatique, École Polytechnique de Montréal, Montréal, Canada H3C 3A7.

IEEE Log Number 9414236.

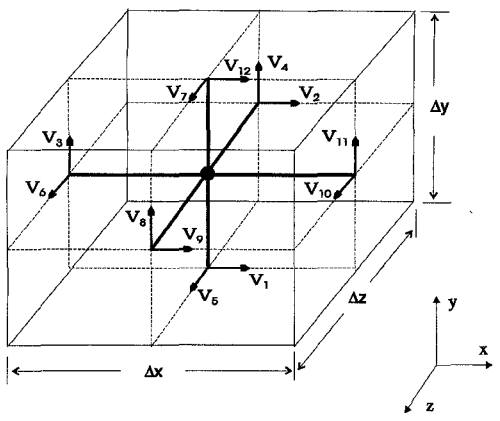

Fig. 1. Space representation of the TLM symmetrical condensed node.

The Maxwell's equations are then formulated in terms of electric and magnetic fields inside the anisotropic material as follows

$$\varepsilon_0\varepsilon_{xx}\frac{\partial E_x}{\partial t}+\varepsilon_0\varepsilon_{xy}\frac{\partial E_y}{\partial t}+\varepsilon_0\varepsilon_{xz}\frac{\partial E_z}{\partial t}=\frac{\partial H_z}{\partial y}-\frac{\partial H_y}{\partial z} \quad (2a)$$

$$\varepsilon_0\varepsilon_{yx}\frac{\partial E_x}{\partial t}+\varepsilon_0\varepsilon_{yy}\frac{\partial E_y}{\partial t}+\varepsilon_0\varepsilon_{yz}\frac{\partial E_z}{\partial t}=\frac{\partial H_x}{\partial z}-\frac{\partial H_z}{\partial x} \quad (2b)$$

$$\varepsilon_0\varepsilon_{zx}\frac{\partial E_x}{\partial t}+\varepsilon_0\varepsilon_{zy}\frac{\partial E_y}{\partial t}+\varepsilon_0\varepsilon_{zz}\frac{\partial E_z}{\partial t}=\frac{\partial H_y}{\partial x}-\frac{\partial H_x}{\partial y} \quad (2c)$$

$$\mu_0\mu_{xx}\frac{\partial H_x}{\partial t}+\mu_0\mu_{xy}\frac{\partial H_y}{\partial t}+\mu_0\mu_{xz}\frac{\partial H_z}{\partial t}=\frac{\partial E_y}{\partial z}-\frac{\partial E_z}{\partial y} \quad (2d)$$

$$\mu_0\mu_{yx}\frac{\partial H_x}{\partial t}+\mu_0\mu_{yy}\frac{\partial H_y}{\partial t}+\mu_0\mu_{yz}\frac{\partial H_z}{\partial t}=\frac{\partial E_z}{\partial x}-\frac{\partial E_x}{\partial z} \quad (2e)$$

$$\mu_0\mu_{zx}\frac{\partial H_x}{\partial t}+\mu_0\mu_{zy}\frac{\partial H_y}{\partial t}+\mu_0\mu_{zz}\frac{\partial H_z}{\partial t}=\frac{\partial E_x}{\partial y}-\frac{\partial E_y}{\partial x}. \quad (2f)$$

Each of these scalar field equations can be transformed into transmission line network (Johns' node). Following Johns' node (Fig. 1) that represents a block of space dimensions, any function of space and time is discretized in terms of graded mesh

$$F^n(i,j,k)=F(i\Delta x, j\Delta y, k\Delta z, n\Delta t) \quad (3)$$

where $\Delta x, \Delta y, \Delta z$ are the grid dimensions and Δt is the time increment. Now the following equality is established that relates network voltages and currents to the electric and magnetic fields

$$\begin{aligned} &V_x=\Delta x\cdot E_x, V_y=\Delta y\cdot E_y, V_z=\Delta z\cdot E_z\\ &I_x=\Delta x\cdot Z_0\cdot H_x/Y_{xx}, I_y=\Delta y\cdot Z_0\cdot H_y/Y_{yy},\\ &I_z=\Delta z\cdot Z_0\cdot H_z/Y_{zz}\\ &X=x/\Delta x, Y=y/\Delta y, Z=z/\Delta z, T=t/\Delta t \end{aligned} \quad (4)$$

where $Y_{xx}=\Delta x\Delta l/\mu_{xx}\Delta y\Delta z, Y_{yy}=\Delta y\Delta l/\mu_{yy}\Delta x\Delta z, Y_{zz}=\Delta z\Delta l/\mu_{zz}\Delta x\Delta y, \Delta t=\Delta l/2c, Z_0$ is the characteristic impedance of free space, Δl is the least dimension of space grids, and c is the velocity of light.

Substituting (4) into (2) leads to a set of coupled differential equations

$$\frac{Y_{exx}+2(Y_{yy}+Y_{zz})}{2}\frac{\partial V_x}{\partial T}+\frac{Y_{exy}}{2}\frac{\partial V_y}{\partial T}+\frac{Y_{exz}}{2}\frac{\partial V_z}{\partial T}=Y_{zz}\frac{\partial I_z}{\partial Y}-Y_{yy}\frac{\partial I_y}{\partial Z} \quad (5a)$$

$$\frac{Y_{eyy}+2(Y_{xx}+Y_{zz})}{2}\frac{\partial V_y}{\partial T}+\frac{Y_{eyx}}{2}\frac{\partial V_x}{\partial T}+\frac{Y_{eyz}}{2}\frac{\partial V_z}{\partial T}=Y_{xx}\frac{\partial I_x}{\partial Z}-Y_{zz}\frac{\partial I_z}{\partial X} \quad (5b)$$

$$\frac{Y_{ezz}+2(Y_{xx}+Y_{yy})}{2}\frac{\partial V_z}{\partial T}+\frac{Y_{ezx}}{2}\frac{\partial V_x}{\partial T}+\frac{Y_{ezy}}{2}\frac{\partial V_y}{\partial T}=Y_{yy}\frac{\partial I_y}{\partial X}-Y_{xx}\frac{\partial I_x}{\partial Y} \quad (5c)$$

$$2\frac{\partial I_x}{\partial T}+\frac{Y_{mxy}}{2}\frac{\partial I_y}{\partial T}+\frac{Y_{mxz}}{2}\frac{\partial I_z}{\partial T}=\frac{\partial V_y}{\partial Z}-\frac{\partial V_z}{\partial Y} \quad (5d)$$

$$2\frac{\partial I_y}{\partial T}+\frac{Y_{myx}}{2}\frac{\partial I_x}{\partial T}+\frac{Y_{myz}}{2}\frac{\partial I_z}{\partial T}=\frac{\partial V_z}{\partial X}-\frac{\partial V_x}{\partial Z} \quad (5e)$$

$$2\frac{\partial I_z}{\partial T}+\frac{Y_{mzx}}{2}\frac{\partial I_x}{\partial T}+\frac{Y_{mzy}}{2}\frac{\partial I_y}{\partial T}=\frac{\partial V_x}{\partial Y}-\frac{\partial V_y}{\partial X} \quad (5f)$$

where

$$\begin{aligned} &Y_{exx}=\frac{4\varepsilon_{xx}}{\mu_{xx}Y_{xx}}-2(Y_{yy}+Y_{zz}),\quad Y_{exy}=\frac{4\Delta z\varepsilon_{xy}}{\Delta l},\\ &Y_{exz}=\frac{4\Delta y\varepsilon_{xz}}{\Delta l},\quad Y_{eyy}=\frac{4\varepsilon_{yy}}{\mu_{yy}Y_{yy}}-2(Y_{xx}+Y_{zz}),\\ &Y_{eyx}=\frac{4\Delta z\varepsilon_{yx}}{\Delta l},\quad Y_{eyz}=\frac{4\Delta x\varepsilon_{yz}}{\Delta l},\\ &Y_{ezz}=\frac{4\varepsilon_{zz}}{\mu_{zz}Y_{zz}}-2(Y_{xx}+Y_{yy}),\quad Y_{ezx}=\frac{4\Delta y\varepsilon_{zx}}{\Delta l},\\ &Y_{ezy}=\frac{4\Delta x\varepsilon_{zy}}{\Delta l},\quad Y_{mxy}=\frac{4\Delta z\mu_{xy}Y_{yy}}{\Delta l},\\ &Y_{myx}=\frac{4\Delta z\mu_{yx}Y_{xx}}{\Delta l},\quad Y_{mzx}=\frac{4\Delta y\mu_{zx}Y_{xx}}{\Delta l},\\ &Y_{mxz}=\frac{4\Delta y\mu_{xz}Y_{zz}}{\Delta l},\quad Y_{myz}=\frac{4\Delta x\mu_{yz}Y_{zz}}{\Delta l},\\ &Y_{mzy}=\frac{4\Delta x\mu_{zy}Y_{yy}}{\Delta l}. \end{aligned}$$

Clearly, (5) can be exactly reduced to the formulation of the hybrid SCN developed in [12], [15] as long as the off-diagonal elements of both permittivity and permeability tensors are vanishing. Note that the equivalent voltages V_x, V_y, V_z and currents I_x, I_y, I_z are normally determined by applying the same procedure as in [17]. As such, a pair of decoupled matrix equations are found to be

$$\begin{bmatrix} Y_{ex} & Y_{exy} & Y_{exz}\\ Y_{eyx} & Y_{ey} & Y_{eyz}\\ Y_{ezx} & Y_{ezy} & Y_{ez}\end{bmatrix}\cdot\begin{bmatrix}V_x\\V_y\\V_z\end{bmatrix}=\begin{bmatrix}\Psi_x\\\Psi_y\\\Psi_z\end{bmatrix} \quad (6a)$$

$$\begin{bmatrix} Y_{mx} & Y_{mxy} & Y_{mxz}\\ Y_{myx} & Y_{my} & Y_{myz}\\ Y_{mzx} & Y_{mzy} & Y_{mz}\end{bmatrix}\cdot\begin{bmatrix}I_x\\I_y\\I_z\end{bmatrix}=\begin{bmatrix}\Phi_x\\\Phi_y\\\Phi_z\end{bmatrix} \quad (6b)$$

in which

$$\Psi_x = 2[Y_{yy}(V_2^i + V_9^i) + Y_{zz}(V_1^i + V_{12}^i) + Y_{exx}V_{13}^i + Y_{exy}V_{14}^i + Y_{exz}V_{15}^i]$$
$$\Psi_y = 2[Y_{xx}(V_4^i + V_8^i) + Y_{zz}(V_3^i + V_{11}^i) + Y_{eyx}V_{13}^i + Y_{eyy}V_{14}^i + Y_{eyz}V_{15}^i]$$
$$\Psi_z = 2[Y_{xx}(V_5^i + V_7^i) + Y_{yy}(V_6^i + V_{10}^i) + Y_{ezx}V_{13}^i + Y_{ezy}V_{14}^i + Y_{ezz}V_{15}^i]$$
$$\Phi_x = 2(V_5^i + V_8^i - V_4^i - V_7^i + Y_{mxy}V_{17}^i + Y_{mxz}V_{18}^i)$$
$$\Phi_y = 2(V_2^i + V_{10}^i - V_6^i - V_9^i + Y_{myx}V_{16}^i + Y_{myz}V_{18}^i)$$
$$\Phi_z = 2(V_3^i + V_{12}^i - V_1^i - V_{11}^i + Y_{mzx}V_{16}^i + Y_{mzy}V_{17}^i)$$
$$Y_{ex} = Y_{exx} + 2(Y_{yy} + Y_{zz}), Y_{ey} = Y_{eyy} + 2(Y_{xx} + Y_{zz})$$
$$Y_{ez} = Y_{ezz} + 2(Y_{xx} + Y_{yy}), Y_{mx} = Y_{my} = Y_{mz} = 4.$$

Solving matrix (6a) and (6b), the equivalent voltages and currents of the node are given by

$$V_x = \frac{1}{\Delta e}(A_{xx}\Psi_x + A_{xy}\Psi_y + A_{xz}\Psi_z) \quad (7a)$$
$$V_y = \frac{1}{\Delta e}(A_{yx}\Psi_x + A_{yy}\Psi_y + A_{yz}\Psi_z) \quad (7b)$$
$$V_z = \frac{1}{\Delta e}(A_{zx}\Psi_x + A_{zy}\Psi_y + A_{zz}\Psi_z) \quad (7c)$$
$$I_x = \frac{1}{\Delta m}(B_{xx}\Phi_x + B_{xy}\Phi_y + B_{xz}\Phi_z) \quad (7d)$$
$$I_y = \frac{1}{\Delta m}(B_{yx}\Phi_x + B_{yy}\Phi_y + B_{yz}\Phi_z) \quad (7e)$$
$$I_z = \frac{1}{\Delta m}(B_{zx}\Phi_x + B_{zy}\Phi_y + B_{zz}\Phi_z) \quad (7f)$$

with

$$A_{xx} = Y_{ey}Y_{ez} - Y_{ezy}Y_{eyz}, \quad A_{xy} = Y_{ezy}Y_{exz} - Y_{exy}Y_{ez},$$
$$A_{xz} = Y_{exy}Y_{eyz} - Y_{ey}Y_{exz}$$
$$A_{yx} = Y_{ezx}Y_{exz} - Y_{eyx}Y_{ez}, \quad A_{yy} = Y_{ex}Y_{ez} - Y_{exz}Y_{ezx},$$
$$A_{yz} = Y_{eyx}Y_{exz} - Y_{ex}Y_{eyz}$$
$$A_{zx} = Y_{eyx}Y_{ezy} - Y_{ey}Y_{ezx}, \quad A_{zy} = Y_{exy}Y_{ezx} - Y_{ezy}Y_{ex},$$
$$A_{zz} = Y_{ex}Y_{ey} - Y_{exy}Y_{eyx}$$
$$B_{xx} = Y_{my}Y_{mz} - Y_{mzy}Y_{myz},$$
$$B_{xy} = Y_{mzy}Y_{mxz} - Y_{mxy}Y_{mz},$$
$$B_{xz} = Y_{mxy}Y_{myz} - Y_{my}Y_{mxz}$$
$$B_{yx} = Y_{mzx}Y_{mxz} - Y_{myx}Y_{mz},$$
$$B_{yy} = Y_{mx}Y_{mz} - Y_{mxz}Y_{mzx},$$
$$B_{yz} = Y_{myx}Y_{mxz} - Y_{mx}Y_{myz}$$
$$B_{zx} = Y_{myx}Y_{mzy} - Y_{my}Y_{mzx},$$
$$B_{zy} = Y_{mxy}Y_{mzx} - Y_{mzy}Y_{mx},$$
$$B_{zz} = Y_{mx}Y_{my} - Y_{mxy}Y_{myx}$$

$$\Delta e = \begin{vmatrix} Y_{ex} & Y_{exy} & Y_{exz} \\ Y_{eyx} & Y_{ey} & Y_{eyz} \\ Y_{ezx} & Y_{ezy} & Y_{ez} \end{vmatrix},$$
$$\Delta m = \begin{vmatrix} Y_{mx} & Y_{mxy} & Y_{mxz} \\ Y_{myx} & Y_{my} & Y_{myz} \\ Y_{mzx} & Y_{mzy} & Y_{mz} \end{vmatrix}.$$

Since the SCN can be represented by three pairs of equivalent shunt and series nodes [18], averaging the appropriate voltages and currents at the center of the node yields six pairs of hybrid equations that interrelate reflected and incident voltages, such as

$$V_1^r = V_x + I_z - V_{12}^i$$
$$V_{12}^r = V_x - I_z - V_1^i \quad (8a)$$
$$V_2^r = V_x - I_y - V_9^i$$
$$V_9^r = V_x + I_y - V_2^i \quad (8b)$$
$$V_3^r = V_y - I_z - V_{11}^i$$
$$V_{11}^r = V_y + I_z - V_3^i \quad (8c)$$
$$V_4^r = V_y + I_x - V_8^i$$
$$V_8^r = V_y - I_x - V_4^i \quad (8d)$$
$$V_5^r = V_z - I_x - V_7^i$$
$$V_7^r = V_z + I_x - V_5^i \quad (8e)$$
$$V_6^r = V_z + I_y - V_{10}^i$$
$$V_{10}^r = V_z - I_y - V_6^i. \quad (8f)$$

The combination of (8) with (7) leads to a generalized 18 × 18 scattering matrix which also takes into account the open- and short-circuit stubs. These stubs are added to account for the cell topology, permittivity and permeability tensors. The matrix consists of a number of explicit elements, such as

$$S_{29} = \frac{2A_{xx}Y_{yy}}{\Delta e} + \frac{2B_{yy}}{\Delta m} - 1.$$

B. Frequency-Domain Algorithm for Eigenvalue Problems

A TLM algorithm based on the proposed node is implemented in the frequency domain. This is to examine the usefulness of the present theory for circuit problems dealing with frequency-dependent permittivity and permeability tensors such as magnetized ferrite. The concept of the frequency domain TLM (FDTLM) has been well established in [10], [13], and [14]. Due to the anisotropic property of material, however, the original eigenvalue equation [10], [13] for waveguiding structures is no longer valid. Some modifications are required with regards to the nonreciprocity under the anisotropic medium in the waveguiding structure.

Under the TLM framework, any waveguiding structure is discretized as an infinitely long periodic network with a periodicity of Δz in the propagation direction. Therefore, the eigenvalue equation is constructed from only one slice of waveguide which contains simply one node in the propagation direction as shown in Fig. 2. In this case, the scattering matrix is given by

$$\begin{bmatrix} b_1 \\ b_2 \end{bmatrix} = \begin{bmatrix} S_{11} & S_{12} \\ S_{21} & S_{22} \end{bmatrix} \cdot \begin{bmatrix} a_1 \\ a_2 \end{bmatrix} \quad (9)$$

where $a_{1,2}$ denotes the incident voltage vector and $b_{1,2}$ the reflected voltage vector. To determine propagation constants and corresponding transverse field profiles of a specific waveguide mode, a transfer matrix A is derived first from the scattering counterpart, such as

$$\begin{bmatrix} V_1 \\ I_1 \end{bmatrix} = [A] \cdot \begin{bmatrix} V_2 \\ I_2 \end{bmatrix} = [A] \cdot \begin{bmatrix} V_1 \\ I_1 \end{bmatrix} \cdot e^{-\gamma \Delta z}. \quad (10)$$

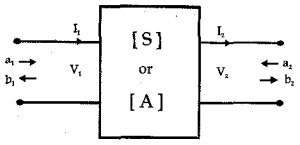

Fig. 2. Network equivalence for a slice of waveguide with a length Δz of in z direction.

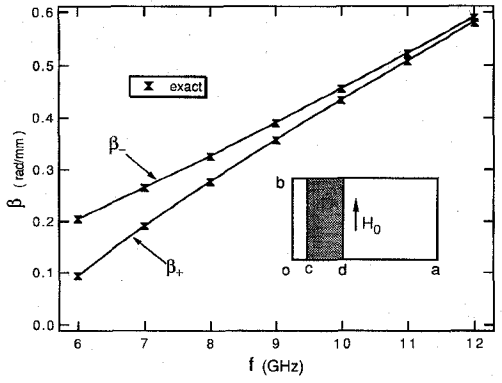

Fig. 3. Phase constant of the TE_{10} mode of a rectangular waveguide loaded with a ferrite slab ($a = 22.86$ mm, $b = 10.16$ mm, $c = 2.286$ mm, $d = 8.0$ mm, $\varepsilon_r = 9.0$, $4\pi M_s = 2000G_s$, $H_o = 200O_e$).

This matrix then yields the characteristic eigenvalue equation

$$A \cdot \begin{bmatrix} V_1 \\ I_1 \end{bmatrix} = \Re \cdot \begin{bmatrix} V_1 \\ I_1 \end{bmatrix}, \quad \Re = e^{\gamma \Delta z}. \tag{11}$$

The propagation constant γ is easily deduced from the eigenvalue $\Re$ and the transverse field profile of mode pertaining to the eigenvalue is obtained by the eigenvector of the matrix A.

III. Numerical Examples

To validate the proposed TLM algorithm in the frequency domain and also its computational accuracy, a variety of waveguiding structures involving complex anisotropic materials are calculated and compared with results from the analytical solution and other numerical techniques available in the literature.

A. Rectangular Waveguide Partially Filled with Magnetized Ferrite

Since a rectangular waveguide containing ferrite with transverse magnetization presents a very simple example for which analytical solutions are available, a comparison can be effectively made to examine and validate the proposed TLM model. In this case, the permeability tensor of a ferrite slab is degenerated to be

$$\overleftrightarrow{\mu} = \mu_0 \cdot \begin{bmatrix} \mu_{xx} & 0 & \mu_{xz} \\ 0 & \mu_{yy} & 0 \\ \mu_{zx} & 0 & \mu_{zz} \end{bmatrix} = \mu_0 \cdot \begin{bmatrix} \mu & 0 & -jk \\ 0 & 1 & 0 \\ jk & 0 & \mu \end{bmatrix} \tag{12}$$

where μ and k are determined in the conventional way [5]. Fig. 3 shows dispersion characteristics of the TE_{10} mode. Even if a coarse mesh (8×4 nodes) is used, the results obtained by the present modeling are in excellent agreement with the exact solutions [5].

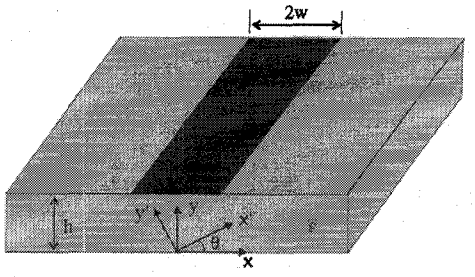

Fig. 4. Microstrip geometry showing the crystal (x', y') and microstrip (x, y) axes.

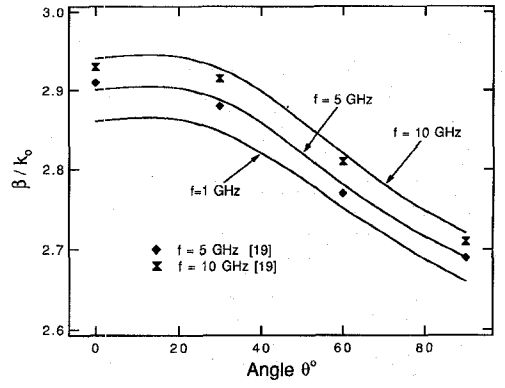

Fig. 5. Normalized propagation constant β/k_o at 1, 5, and 10 GHz obtained by the present model for microstrip lines deposited on the m-cut sapphire as a function of the rotation angle θ of the optic axis. A comparison is made between [19] and this technique for $w = h = 0.5$ mm.

B. Microstrip on m-cut Sapphire Substrate

A microstrip line is deposited on the m-cut sapphire substrate as shown in Fig. 4. Suppose that the principal axes (x', y') of the sapphire substrate form an angle θ with respect to the microstrip coordinate system (x, y). The relative permittivity tensor are given in the microstrip coordinate system by

$$\overleftrightarrow{\varepsilon} = \begin{bmatrix} \varepsilon_{xx} & \varepsilon_{xy} & 0 \\ \varepsilon_{yx} & \varepsilon_{yy} & 0 \\ 0 & 0 & \varepsilon_{zz} \end{bmatrix}. \tag{13}$$

The elements of above $\overleftrightarrow{\varepsilon}$ are calculated by the following analytical equations

$$\begin{aligned} \varepsilon_{xx} &= \varepsilon_1 \cos^2 \theta + \varepsilon_2 \sin^2 \theta \\ \varepsilon_{yy} &= \varepsilon_1 \sin^2 \theta + \varepsilon_2 \cos^2 \theta \\ \varepsilon_{xy} &= \varepsilon_{yx} = (\varepsilon_1 - \varepsilon_2) \sin \theta \cos \theta \\ \varepsilon_{zz} &= \varepsilon_1. \end{aligned} \tag{14}$$

With reference to [19], the parameters of structure are defined by $\varepsilon_1 = 9.4, \varepsilon_2 = 11.6, w = h = 0.5$ mm. Fig. 5 illustrates the frequency-dependent characteristics of β/k_0. A comparison between two different approaches is made and shows a good agreement.

C. Microstrip on r-cut Sapphire Substrate

The sapphire material presents an excellent candidate for substrate use of high-temperature superconducting circuits [1],

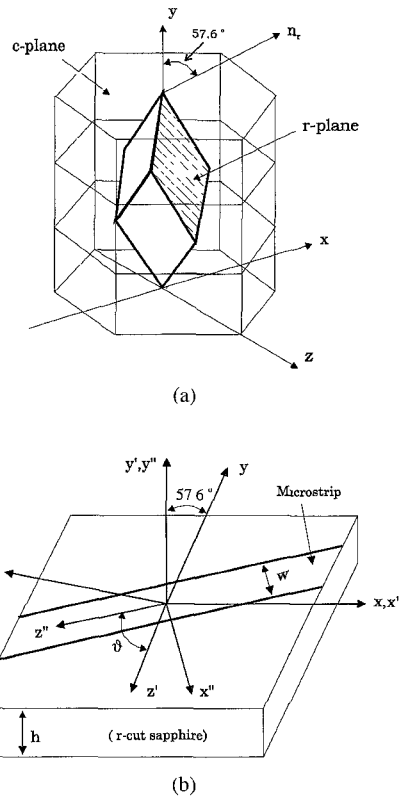

Fig. 6. (a) Morphological hexogonal unit cell of sapphire. (b) Arbitrarily oriented r-cut sapphire-based microstrip.

TABLE I
THE TENSOR ELEMENTS DESCRIBED IN EQUATION (19) AS A FUNCTION OF THE ARBITRARILY ORIENTED ROTATION ANGLE ϑ

ϑ	ε_{xx}	ε_{yy}	ε_{zz}	ε_{xy}	ε_{xz}	ε_{yz}
0°	10.97	10.03	9.40	-0.99	0	0
22.5°	10.74	10.03	9.63	-0.92	0.55	-0.38
45°	10.18	10.03	10.18	-0.70	0.78	-0.70
67.5°	9.63	10.03	10.74	-0.38	0.55	-0.92
90°	9.40	10.03	10.97	0	0	-0.99
112.5°	9.63	10.03	10.74	0.38	-0.55	-0.92
135°	10.18	10.03	10.18	0.70	-0.78	-0.70
157.5°	10.74	10.03	9.63	0.92	-0.55	-0.38
180°	10.97	10.03	9.40	0.99	0	0

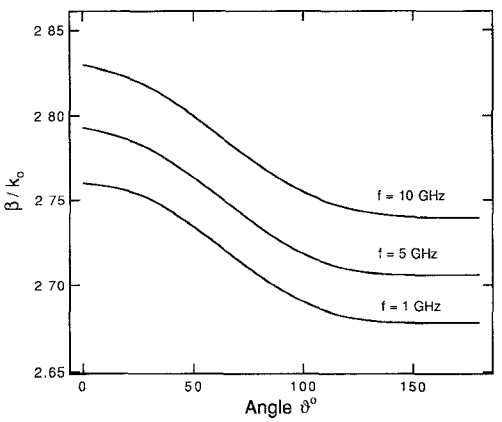

Fig. 7. Propagation characteristics at 1, 5, and 10 GHz for a microstrip line deposited on the r-cut sapphire as a function of the arbitrarily oriented rotation angle ϑ ($w = h = 0.5$ mm).

[2]. This is mainly attributed to its low dielectric loss, excellent thermal coefficient, rigid mechanical strength, and low dielectric permittivity. There are models available for the z-cut and m-cut microstrips [20]. It has been recently suggested that the r-cut microstrip be more attractive for superconductive circuits [21]. However, the analysis of such a structure becomes very tedious because of the tensor complexity. Quasi-static characteristics were given in [21] as functions of the strip geometry and its orientation on the surface of the substrate. To obtain the tensor under the Cartesian, both the morphological hexagonal unit cell of sapphire and the arbitrarily oriented r-cut based microstrip are shown in Fig. 6 [21]. The dielectric permittivity tensor of the sapphire in the principal axis of the crystal is given by

$$\overleftrightarrow{\varepsilon}^{0} = \begin{bmatrix} 9.4 & 0 & 0 \\ 0 & 11.6 & 0 \\ 0 & 0 & 9.4 \end{bmatrix}. \tag{15}$$

A transformation of this tensor for the r-cut ($\theta = 57.6°$) sapphire is done with the operator $\overleftrightarrow{U}_r$

$$\overleftrightarrow{U}_r = \begin{bmatrix} 1 & 0 & 0 \\ 0 & \cos\theta & \sin\theta \\ 0 & -\sin\theta & \cos\theta \end{bmatrix}. \tag{16}$$

The new tensor in (x', y', z') coordinates is

$$\overleftrightarrow{\varepsilon}' = \overleftrightarrow{U}_r \cdot \overleftrightarrow{\varepsilon}^{0} \cdot \overleftrightarrow{U}_r^{-1} = \begin{bmatrix} 9.4 & 0 & 0 \\ 0 & 10.03 & -0.99 \\ 0 & -0.99 & 10.97 \end{bmatrix}. \tag{17}$$

Given an arbitrarily oriented microstrip (Fig. 6(b)), a rotation around the y'-axis of the substrate through the angle ϑ is performed with the operator $\overleftrightarrow{U}_0$, which leads to

$$\overleftrightarrow{U}_0 = \begin{bmatrix} \cos\vartheta & 0 & \sin\vartheta \\ 0 & 1 & 0 \\ -\sin\vartheta & 0 & \cos\vartheta \end{bmatrix}. \tag{18}$$

The final tensor in (x'', y'', z'') coordinates is

$$\overleftrightarrow{\varepsilon}'' = \begin{bmatrix} \varepsilon_{xx} & \varepsilon_{xy} & \varepsilon_{xz} \\ \varepsilon_{yx} & \varepsilon_{yy} & \varepsilon_{yz} \\ \varepsilon_{zx} & \varepsilon_{zy} & \varepsilon_{zz} \end{bmatrix} \tag{19}$$

in which $\varepsilon_{xy} = \varepsilon_{yx}, \varepsilon_{xz} = \varepsilon_{zx}, \varepsilon_{yz} = \varepsilon_{zy}$. The elements of this tensor as a function of the angle ϑ are given in the Table I. Fig. 7 shows normalized propagation constants against the angle ϑ of the r-cut based microstrip line with $w/h = 2$ at different frequencies. It indicates that the influence of the angle ϑ on dispersion characteristics is more pronounced between $\vartheta = 45°$ and $\vartheta = 90°$. On the other hand, the frequency dependency seems to be linear for a given angle ϑ. Since the superconductive microstrip line based on the r-cut sapphire may find applications at higher frequencies going into millimeter-wave range, it is absolutely imperative to consider the dispersion effect under such an anisotropic condition.

IV. CONCLUSION

In this paper, a generalized TLM node has been derived under the condition of both permittivity and permeability tensors.

A TLM algorithm in the frequency domain using the proposed node is developed and used to calculate eigenvalue problems of waveguiding structures involving arbitrary anisotropic properties. A number of examples using complex tensors verify the present theory and demonstrate its usefulness. In particular, frequency-dependent characteristics of r-cut sapphire-based microstrips are obtained. It is believed that the present tool paves the way for field-theoretical design and optimization of high-Tc superconducting microwave devices. On this basis, it is concluded that a unified TLM solver can be made to analyze, design, and optimize a large class of complex structures ranging from microwave circuits to optical devices.

REFERENCES

[1] B. F. Cole, G. C. Liang, N. Newman, K. Char, G. Zaharchuk, and J. S. Martens, "Large-area $YBa_2Cu_3O_{7-d}$ thin films on sapphire for microwave applications," *Appl. Phys. Lett.*, vol. 61, no. 14, pp. 1727–1729, 1992.

[2] J. Gao, B. B. G. Klopman, W. A. Aarnik, A. E. Reitsma, G. J. Gerrittsma, and H. Rogalla, "Epitaxial $YBa_2Cu_3O_7$ thin films on sapphire with Pr $YBa_2Cu_3O_x$ buffer layer," *J. Appl. Phys.*, vol. 71, no. 5, pp. 2333–2337, 1992.

[3] H. Nishihara, M. Haruna, and T. Suhara, *Optical Integrated Circuits.* New York: McGraw-Hill, 1989.

[4] R. C. Alferness, "Waveguide electro-optic modulators," *IEEE Trans. Microwave Theory Tech.*, vol. MTT-30, pp. 1137–1221, Aug. 1982.

[5] B. Lax and K. J. Button, *Microwave Ferrites and Ferrimagnetics.* New York: McGraw-Hill, 1962.

[6] P. B. Johns and R. L. Beurle, "Numerical solution of 2-dimensional scattering problems using a transmission-line matrix," *Proc. Inst. Elec. Eng.*, vol. 118, no. 9, pp. 1203–1208, Sept. 1971.

[7] P. Saguet and E. Pic, "Un traitement du signal simple four ameliorer la methode TLM," *Electron. Lett.*, vol. 16, pp. 247–248, Mar. 1980.

[8] W. J. R. Hoefer, "The transmission line matrix method—Theory and application," *IEEE Trans. Microwave Theory Tech.*, vol. MTT-33, pp. 882–893, Oct. 1985.

[9] ——, "Time-domain electromagnetic simulation for microwave CAD applications," *IEEE Trans. Microwave Theory Tech.*, vol. 40, pp. 1517–1527, July 1992.

[10] H. Jin and R. Vahldieck, "The frequency domain transmission line matrix method—A new concept," *IEEE Trans. Microwave Theory Tech.*, vol. 40, pp. 2207–2218, Dec. 1992.

[11] P. B. Johns, "A symmetrical condensed node for the TLM method," *IEEE Trans. Microwave Theory Tech.*, vol. MTT-35, pp. 370–377, Apr. 1987.

[12] R. A. Scaramuzza and A. J. Lowery, "Hybrid symmetrical condensed node for the TLM method," *Electron. Lett.*, vol. 26, pp. 1947–1949, 1990.

[13] J. Huang, R. Vahldieck, and H. Jin, "Fast frequency domain TLM analysis of 3D circuit discontinuity," in *9th Annual Rev. of Prog. in Applied Comp. in EM,* Mar. 1993, pp. 475–481.

[14] D. P. Johns, A. J. Wlodarczyk, A. Mallik, and C. Christopoulos, "New TLM technique for steady-state field solutions in three dimensions," *Electron. Lett.*, vol. 29, no. 18, pp. 1692–1694, 1992.

[15] P. Berini and K. Wu, "A pair of hybrid symmetrical condensed TLM nodes," *IEEE Microwave and Guided Wave Lett.*, vol. 4, pp. 244–246, July 1994.

[16] J. Huang, K. Wu, P. Morin, and C. Akyel, "Electromagnetic analysis of composite coaxial cells for wideband measurements of highly dispersive materials," to be published in *1995 IEEE MTT-S Int. Microwave Symp. Dig.*

[17] H. Jin, R. Vahldieck, and J. Huang, "Direct derivation of the TLM symmetrical condensed node from Maxwell's equation using centered differencing and averaging," in *1994 IEEE MTT-S Int. Microwave Symp. Dig.*, pp. 23–26.

[18] J. L. Herring and C. Christopoulos, "The application of different meshing techniques to EMC problems," in *9th Annual Rev. of Prog. Appl. Comp. in EM,* Mar. 1993, pp. 755–762.

[19] J. L. Tsalamengas, N. K. Uzunoglu, and N. G. Alexopoulos, "Propagation characteristics of a microstrip line printed on a general anisotropic substrate," *IEEE Trans. Microwave Theory Tech.*, vol. MTT-33, pp. 941–945, Oct. 1985.

[20] L. H. Lee, W. J. Lyons, T. P. Orlando, S. M. Ali, and R. S. Withers, "Full-wave analysis of superconducting microstrip lines on anisotropic substrates using equivalent impedance approach," *IEEE Trans. Microwave Theory Tech.*, vol. 41, pp. 2359–2367, Dec. 1993.

[21] I. B. Vendik, O. G. Vendik, and S. S. Gevorgian, "Effective dielectric permittivity of r-cut sapphire microstrip," in *24th European Microwave Conf. Proc.*, 1994, pp. 395–400.

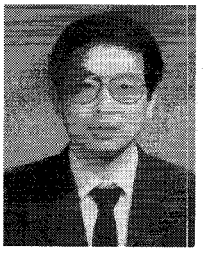

Jifu Huang received the B.Eng. and M.Eng. degrees in radio engineering from Nanjing Institute of Technology (now Southeast University), Nanjing, China, in 1982 and 1987, respectively. From 1991 to 1994, he studied for Ph.D. degree in the Department of Electrical and Computer Engineering, University of Victoria, B.C., Canada.

He joined the faculty of engineering at Southeast University in 1982, where he worked as a Research and Teaching Assistant, and from 1987 to 1991 as a Lecturer. Since April 1994, he has been a Postdoctoral Fellow at the Research Center for Advanced Microwave and Space Electronics, Ecole Polytechnique of Montreal, Canada. His current research interest is in numerical modeling and CAD of microwave/millimeter wave integrated circuits for communications.

Ke Wu (M'87–SM'92) was born in Jiangsu, China. He received the B.Sc. degree (with distinction) in radio engineering from Nanjing Institute of Technology (now Southeast University), Nanjing, China, and the D.E.A. degree in electronics and Ph.D. degree (with distinction) in optics, optoelectronics, and microwave engineering from Institut National Polytechnique de Grenoble (INPG), France.

From 1983 to 1987, he conducted research in the Laboratoire d'Eléctromagnetisme, Microondes et Optoélectronics (LEMO), Grenoble, France. From 1988 to 1992 he was a Research Associate at the University of Victoria, Victoria, B.C., Canada. In 1992, he joined the Département de Génie Électrique et de Génie Informatique at the École Polytechnique de Montréal as an Assistant Professor. His current research interests include analysis and design of various microwave/millimeter-wave integrated circuits and antennas, high-speed interconnects and packaging effects, numerical methods, dielectric material characterizations and superconducting devices. He is also interested in research and design of broadband optoelectronic components and lightwave transmission systems with emphasis on traveling-wave electro-optic modulators, couplers and switches. He has published more than 100 papers.

Dr. Wu received a U.R.S.I. Young Scientist Award in 1987, and, together with two coauthors, the Oliver Lodge Premium from the IEE in 1988. He serves on editorial or review boards of various technical journals.